Astronomy & Astrophysics manuscript no. main
March 21, 2024

Resistively controlled primordial magnetic turbulence decay

A. Brandenburg[1,2,3,4,5], A. Neronov[6,7], and F. Vazza[8,9,10]

[1] Nordita, KTH Royal Institute of Technology and Stockholm University, Hannes Alfvéns väg 12, 10691 Stockholm, Sweden
[2] The Oskar Klein Centre, Department of Astronomy, Stockholm University, AlbaNova, 10691 Stockholm, Sweden
[3] McWilliams Center for Cosmology & Department of Physics, Carnegie Mellon University, 5000 Forbes Ave, Pittsburgh, PA 15213, USA
[4] School of Natural Sciences and Medicine, Ilia State University, 3-5 Cholokashvili Avenue, 0194 Tbilisi, Georgia
[5] Department of Astrophysics, American Museum of Natural History, 200 Central Park West, New York, NY 10024, USA
[6] Astroparticules et Cosmologie, Université Paris Cité, CNRS, Astroparticule et Cosmologie, 75006 Paris, France
[7] Laboratory of Astrophysics, École Polytechnique Fédérale de Lausanne, 1015 Lausanne, Switzerland
[8] Dipartimento di Fisica e Astronomia, Universita di Bologna, Via Gobetti 93/2, 40129 Bologna, Italy
[9] INAF Istituto di Radioastronomia, Via P. Gobetti 101, 40129 Bologna, Italy
[10] Hamburger Sternwarte, Universität Hamburg, Gojenbergsweg 112, 41029 Hamburg, Germany

March 21, 2024

ABSTRACT

Context. Magnetic fields generated in the early Universe undergo turbulent decay during the radiation-dominated era. The decay is governed by a decay exponent and a decay time. It has been argued that the latter is prolonged by magnetic reconnection, which depends on the microphysical resistivity and viscosity. Turbulence, on the other hand, is not usually expected to be sensitive to microphysical dissipation, which affects only very small scales.
Aims. We want to test and quantify the reconnection hypothesis in decaying hydromagnetic turbulence.
Methods. We perform high-resolution numerical simulations with zero net magnetic helicity using the Pencil Code with up to 2048^3 mesh points and relate the decay time to the Alfvén time for different resistivities and viscosities.
Results. The decay time is found to be longer than the Alfvén time by a factor that increases with increasing Lundquist number to the 1/4 power. The decay exponent is as expected from the conservation of the Hosking integral, but a timescale dependence on resistivity is unusual for developed turbulence and not found for hydrodynamic turbulence. In two dimensions, the Lundquist number dependence is shown to be leveling off above values of $\approx 25,000$, independently of the value of the viscosity.
Conclusions. Our numerical results suggest that resistivity effects have been overestimated by Hosking and Schekochihin in their recent work to reconcile the cosmic void observations with primordial magnetogenesis. Instead of reconnection, it may be the magnetic helicity density in smaller patches that is responsible for the resistively slow decay. The leveling off at large Lundquist number cannot currently be confirmed in three dimensions.

Key words. magnetic reconnection – turbulence – magnetohydrodynamics (MHD) – hydrodynamics

1. Introduction

The study of decaying turbulence plays an important role in the early Universe during the radiation-dominated era, when the magnetic field is well coupled to the plasma. While turbulence speeds up the decay, it can also lead to a significant increase in the typical length scale, which could then be many times larger than the comoving horizon scale at the time of magnetic field generation (Brandenburg et al. 1996; Christensson et al. 2001; Banerjee & Jedamzik 2004). This is important, because magnetogenesis processes during the electroweak era, when the age of the Universe was just a few picoseconds (Vachaspati 1991; Cheng & Olinto 1994; Baym et al. 1996), tend to produce magnetic fields of very small length scales of the order of 1 AU or less.

From the study of decaying hydrodynamic turbulence, it has been known for a long time that turbulent energy density and length scale evolve like power laws (Batchelor 1953; Saffman 1967). The exponents depend on the physics of the decay, specifically on the possibility of a conserved quantity that governs the decay, for example magnetic helicity in the hydromagnetic case (Hatori 1984; Biskamp & Müller 1999). The endpoints of the evolution, however, depend on the relevant timescale, which is traditionally just taken to be the turnover or, in the magnetic case that we consider here, the Alfvén time (Banerjee & Jedamzik 2004). More recently, Hosking & Schekochihin (2023) argued that the turnover time should be replaced by the reconnection time, which could be significantly (up to $10^{5.5}$ times) longer. This would result in an endpoint where the magnetic field strength is larger and the turbulent length scale smaller than otherwise, when the decay time is just the Alfvén time.

One of the hallmarks of turbulence is the fact that its large-scale properties are nearly independent of viscosity and resistivity, which act predominantly on the smallest scales of the system. On the other hand, magnetic reconnection is a process that could potentially limit the speed of the inverse cascade. This idea has been invoked by Hosking & Schekochihin (2023) to explain a premature

termination of the decay process by the time of recombination of the Universe, when its age was about 400,000 years.

The purpose of our paper is to analyze numerical simulations with respect to their decay times at different values of the resistivity. In Sect. 2, we discuss the decay time and its relation to other quantities. In Sect. 3, we present our numerical simulation setup and show the results for a resistivity-dependent decay in Sect. 4. We then compare with a purely hydrodynamic decay in Sect. 5 and with the two-dimensional (2–D) hydromagnetic case in Sect. 6, before concluding in Sect. 8. In Appendix A, we provide a historical note on the anastrophy, i.e., the mean squared magnetic vector potential, and in Appendix B, we show detailed convergence tests for some of our 2–D results.

2. Decay and turnover times

In the following, we focus on the decay of magnetic field. Magnetically dominated turbulence is characterized by the turbulent magnetic energy density $\mathcal{E}_{\rm M}$ and the magnetic integral scale $\xi_{\rm M}$. Both $\mathcal{E}_{\rm M}(t)$ and $\xi_{\rm M}(t)$ can be defined in terms of the magnetic energy spectrum $E_{\rm M}(k,t)$ such that $\mathcal{E}_{\rm M}=\int E_{\rm M}\,{\rm d}k$ and $\xi_{\rm M}=\int k^{-1}E_{\rm M}\,{\rm d}k/\mathcal{E}_{\rm M}$. In decaying turbulence, both quantities depend algebraically rather than exponentially on time. Therefore, the decay is primarily characterized by power laws,

$$\mathcal{E}_{\rm M}\propto t^{-p}\quad\text{and}\quad\xi_{\rm M}\propto t^{q},\tag{1}$$

rather than by exponential laws of the type $\mathcal{E}_{\rm M}\propto e^{-t/\tau}$. The algebraic decay is mainly a consequence of nonlinearity. On the other hand, in decaying hydromagnetic turbulence with significant cross helicity, for example, the nonlinearity in the induction equation is reduced and then the decay is indeed no longer algebraic, but closer to exponential; see Brandenburg & Oughton (2018).

An obvious difference between algebraic and exponential decays is that in the former, $\mathcal{E}_{\rm M}(t)$ is characterized by the nondimensional quantity p, while in the latter, it is characterized by the dimensionful quantity τ. Following Hosking & Schekochihin (2023), a decay time τ can also be defined for an algebraic decay and is then given by

$$\tau^{-1}=-{\rm d}\ln\mathcal{E}_{\rm M}/{\rm d}t.\tag{2}$$

In the present case of a power-law decay, this value of $\tau=\tau(t)$ is time-dependent and can be related to the instantaneous decay exponent

$$p(t)=-{\rm d}\ln\mathcal{E}_{\rm M}/{\rm d}\ln t\tag{3}$$

through $\tau=t/p(t)$, i.e., no new parameter emerges, except for t itself. However, a useful way of incorporating new information is by relating τ to the Alfvén time $\tau_{\rm A}=\xi_{\rm M}/v_{\rm A}$ through

$$\tau=C_{\rm M}\xi_{\rm M}/v_{\rm A},\tag{4}$$

where $C_{\rm M}$ is a non-dimensional parameter, and $v_{\rm A}$ is the Alfvén velocity, which is related to the magnetic energy density through $\mathcal{E}_{\rm M}=B_{\rm rms}^2/2\mu_0=\rho v_{\rm A}^2/2$, where ρ is the density, μ_0 the vacuum permeability, and $B_{\rm rms}$ the root-mean-square (rms) magnetic field.

As was stressed by Hosking & Schekochihin (2023), Eq. (4), can be used to define the endpoints of the evolutionary tracks in a diagram of $B_{\rm rms}$ versus $\xi_{\rm M}$, or, equivalently, $v_{\rm A}$ versus $\xi_{\rm M}$, i.e., $v_{\rm A}=v_{\rm A}(\xi)$. They also emphasized that the location of these endpoints is sensitive to whether or not $C_{\rm M}$ depends on the resistivity of the plasma. If it does depend on the resistivity, this could be ascribed to the effects of magnetic reconnection, which might slow down the turbulent decay.

Magnetic reconnection refers to a change of magnetic field line connectivity that is subject to topological constraints. A standard example is x-point reconnection (see, e.g., Craig & McClymont 1991; Craig et al. 2005), which becomes slower as the x-point gets degenerated into an extremely elongated structure (Sweet 1958; Parker 1957); see Liu et al. (2022) for a review. It is usually believed that in the presence of turbulence, such structures break up into progressively smaller ones, which makes reconnection eventually fast, i.e., independent of the microphysical resistivity (Galsgaard & Nordlund 1996; Lazarian & Vishniac 1999; Comisso & Sironi 2019). However, whether this would also imply that τ becomes independent of the resistivity, remains an unclear issue. For example, Galsgaard & Nordlund (1996) found that resistive heating becomes independent of the value of the resistivity. Another question concerns the speed at which magnetic flux can be processed through a current sheet (Kowal et al. 2009; Loureiro et al. 2012). Also of interest is of course the timescale on which the topology of the magnetic field changes (Lazarian et al. 2020). These different timescales may not all address the value of $C_{\rm M}$ that relates the decay time to the Alfvén time.

In magnetically dominated turbulence, the effect of the resistivity is quantified by the Lundquist number. For decaying turbulence, it is time-dependent and defined as

$${\rm Lu}(t)=v_{\rm A}(t)\,\xi_{\rm M}(t)/\eta.\tag{5}$$

This quantity is similar to the magnetic Reynolds number if we replace $v_{\rm A}$ by the rms velocity, $u_{\rm rms}$. Here, however, the plasma is driven by the Lorentz force, so the Lundquist number is a more direct way of quantifying the resistivity than the magnetic Reynolds number. The Alfvénic Mach number is defined as ${\rm Ma}_{\rm A}=u_{\rm rms}/v_{\rm A}$.

In addition to varying η, we also vary ν such that the magnetic Prandtl number ${\rm Pr}_{\rm M}=\nu/\eta$ is typically in the range $1\leq{\rm Pr}_{\rm M}\leq5$. It is then also convenient to define the Lundquist number based on the reconnection outflow,

$${\rm Lu}_\nu(t)={\rm Lu}(t)/\sqrt{1+{\rm Pr}_{\rm M}}\,;\tag{6}$$

see Hosking & Schekochihin (2023) for details.

3. Numerical simulations

We perform simulations of the compressible hydromagnetic equations for the magnetic vector potential $\boldsymbol{A}$, the velocity $\boldsymbol{u}$, and the logarithmic density $\ln\rho$ in the presence of viscosity ν and magnetic diffusivity η, i.e.,

$$\frac{\partial\boldsymbol{A}}{\partial t}=\boldsymbol{u}\times\boldsymbol{B}+\eta\nabla^2\boldsymbol{A},\tag{7}$$

$$\frac{{\rm D}\boldsymbol{u}}{{\rm D}t}=\frac{1}{\rho}\left[\boldsymbol{J}\times\boldsymbol{B}+\boldsymbol{\nabla}\cdot(2\rho\nu\mathbf{S})\right]-c_{\rm s}^2\boldsymbol{\nabla}\ln\rho,\tag{8}$$

$$\frac{{\rm D}\ln\rho}{{\rm D}t}=-\boldsymbol{\nabla}\cdot\boldsymbol{u},\tag{9}$$

Table 1. Summary of magnetohydrodynamic simulations analyzed in this paper. The time unit of τ_ξ and $\tau_\mathcal{E}$ is $[t] = (c_{\rm s}k_1)^{-1}$.

Run	$\eta k_1/c_{\rm s}$	$\nu k_1/c_{\rm s}$	$\mathrm{Pr_M}$	Lu	Lu_ν	$C_{\rm M}$	$C_{\rm L}^{(1/4)}$	C_ξ	$C_\mathcal{E}$	τ_ξ	$\tau_\mathcal{E}$	$\epsilon_{\rm K}/\epsilon_{\rm M}$	$\mathrm{Ma_A}$	N^3
M0	4×10^{-7}	4×10^{-6}	10	5600	1700	34.4 ± 0.8	4.0	90	0.38	0.79	0.27	1.0	0.21	2048^3
M1	4×10^{-7}	2×10^{-6}	5	5830	2600	30.5 ± 0.8	3.5	87	0.35	0.72	0.23	0.9	0.24	2048^3
M2	1×10^{-6}	2×10^{-6}	2	2354	1660	26.2 ± 0.3	3.8	81	0.32	0.63	0.20	0.6	0.28	2048^3
M3	1×10^{-6}	5×10^{-6}	5	2186	980	25.6 ± 0.6	3.7	80	0.32	0.74	0.22	0.8	0.25	1024^3
M4	2.5×10^{-6}	5×10^{-6}	2	823	580	20.1 ± 0.5	3.7	73	0.27	0.61	0.17	0.6	0.31	1024^3
M5	5×10^{-6}	5×10^{-6}	1	386	386	14.5 ± 0.7	3.3	64	0.23	0.45	0.12	0.5	0.38	1024^3

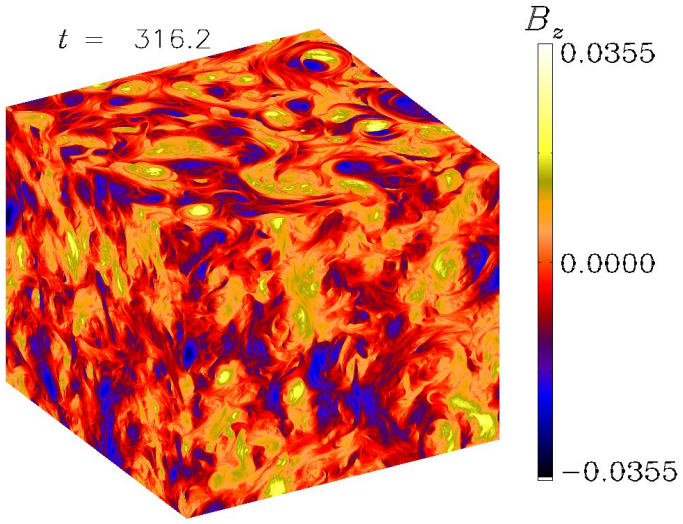

Fig. 1. Visualization of B_z on the periphery of the computational domain for Run M1, where $\mathrm{Pr_M} = 5$.

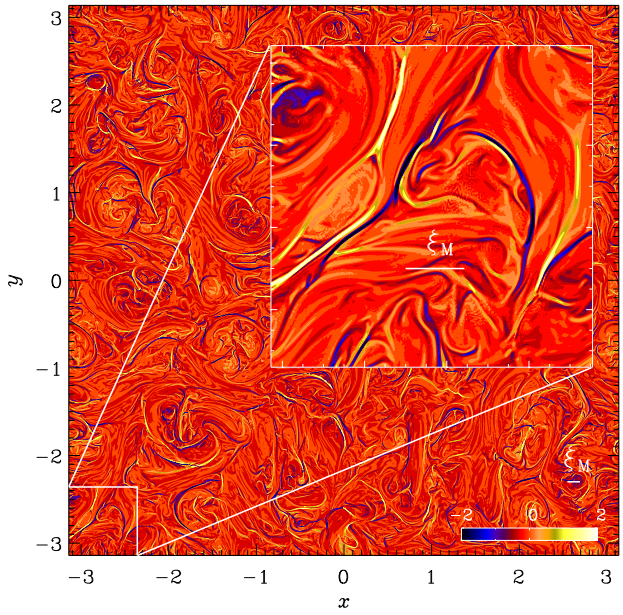

Fig. 2. Visualization of J_z at $z = \pi$ along with a zoom-in on the lower left corner for Run M0, where $\mathrm{Pr_M} = 10$, at $t = 318$. The value of $\xi_{\rm M}$ at that time is indicated by the length of the short white lines.

using as initial condition a random magnetic field such that $E_{\rm M}(k,0)$ has a k^4 subinertial range for $k < k_{\rm p}$ (Durrer & Caprini 2003), and a k^{-2} inertial range for $k > k_{\rm p}$ (Brandenburg et al. 2015). In all cases, we choose $k_{\rm p}/k_1 = 60$, where $k_1 = 2\pi/L$ is the smallest wavenumber in our cubic domain of size L^3. In Eqs. (7) and (8), $\boldsymbol{B} = \boldsymbol{\nabla}\times\boldsymbol{A}$ is the magnetic field, $\boldsymbol{J} = \boldsymbol{\nabla}\times\boldsymbol{B}/\mu_0$ is the current density, and $\mathsf{S}_{ij} = (\partial_i u_j + \partial_j u_i)/2 - \delta_{ij}\boldsymbol{\nabla}\cdot\boldsymbol{u}/3$ are the components of the rate-of-strain tensor S. There is no magnetic helicity on average, but the fluctuations in the local magnetic helicity density $h = \boldsymbol{A}\cdot\boldsymbol{B}$ lead to a decay behavior where the correlation integral of h, which is also known as the Hosking integral, is conserved (Hosking & Schekochihin 2021; Schekochihin 2022; Zhou et al. 2022). We use the Pencil Code (Pencil Code Collaboration et al. 2021), which has also been used for many earlier simulations of decaying hydromagnetic turbulence (Zhou et al. 2022; Brandenburg et al. 2023). All our simulations are in the magnetically dominated regime, because the velocity is just a consequence of and driven by the magnetic field.

Because the magnetic field is initially random, the resulting velocity is also random and it drives a forward turbulent cascade with kinetic and magnetic energy dissipation rates $\epsilon_{\rm K} = \langle 2\nu\rho\mathsf{S}^2\rangle$ and $\epsilon_{\rm M} = \langle\eta\mu_0\boldsymbol{J}^2\rangle$. Their ratio scales with $\mathrm{Pr_M^{1/3}}$ (Brandenburg 2014; Galishnikova et al. 2022). If $k_{\rm p}/k_1$ is large (we recall that we use the value 60), there is also an inverse cascade (Brandenburg et al. 2015). The inverse cascade was also found in the relativistic regime (Zrake 2014) and is now understood to be a consequence of the conservation of the Hosking integral (Hosking & Schekochihin 2021; Schekochihin 2022; Zhou et al. 2022). However, the role played by the Hosking integral is currently not universally accepted (Armua et al. 2023; Dwivedi et al. 2024). The lack of numerical support could be related to insufficiently large values of $k_{\rm p}/k_1$.

We define the kinetic energy spectrum $E_{\rm K}(k,t)$ analogously to $E_{\rm M}(k,t)$, using the normalization $\int E_{\rm K}(k,t)\,{\rm d}k = \mathcal{E}_{\rm K}(t) \equiv \rho_0 u_{\rm rms}^2/2$, where $\rho_0 = \langle\rho\rangle = $ const owing to mass conservation. In magnetically driven turbulence, $\mathcal{E}_{\rm K}$ is about one tenth of $\mathcal{E}_{\rm M} = B_{\rm rms}^2/2\mu_0$, which seems to be surprisingly independent of the physical input parameters (Brandenburg et al. 2017).

In Table 1, we summarize the results of five simulations, Runs M0–M5, where we vary η and ν, as well as the number of mesh points, N^3. We also present some relevant output parameters that will be defined below. They are all obtained from a statistically steady stretch of our time series data, and error bars have been calculated as the largest departure

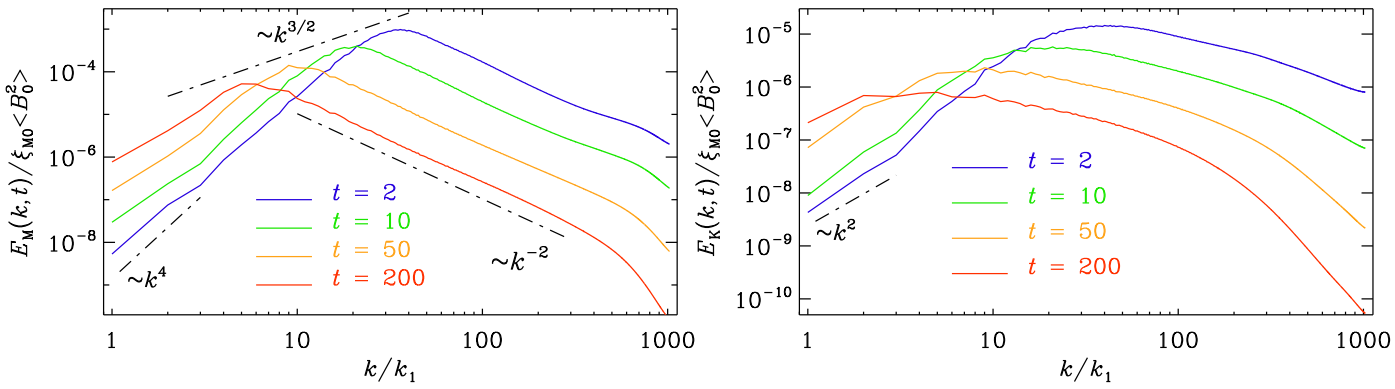

Fig. 3. Magnetic and kinetic energy spectra for Run M1 at different times. Note the k^{-2} inertial range for large values of k. The $\propto k^4$ and $\propto k^2$ slopes are indicated for reference. As elsewhere, time is in unit of $[t] = (c_s k_1)^{-1}$.

from any one third of the time series. A visualization of the z components of $\boldsymbol{B}$ on the periphery of the computational domain for Run M1 is shown in Fig. 1. Figure 2 shows J_z in an xy plane together with a zoom-in on the lower left corner of the domain. The corresponding magnetic and kinetic energy spectra are shown in Fig. 3 for different times in units of $[t] = (c_s k_1)^{-1}$.

The $E_M(k,t) \propto k^{-2}$ inertial range can be explained by weak turbulence scaling (Brandenburg et al. 2015), but it becomes a bit shallower near the dissipation subrange. This could follow from some kind of magnetic bottleneck effect associated with reconnection, analogously to the bottleneck effect in hydrodynamic turbulence (Falkovich 1994).

Note that at late times, the subinertial range spectrum of $E_M(k,t)$ becomes shallower than the initial k^4 slope. This is an artifact of poor scale separation; see Brandenburg et al. (2023) for related numerical evidence. On the other hand, a k^2 subinertial range for $E_K(k,t)$ has been seen for some time; see Kahniashvili et al. (2013).

In our numerical simulations, we use units such that $c_s = k_1 = \rho_0 = \mu_0 = 1$. The resistivity, $\mu_0\eta$, is therefore the same as the magnetic diffusivity. Nevertheless, most of the results below are expressed in manifestly nondimensional form.

4. Resistivity-dependent decay

We now analyze a collection of runs similar to those of the recent works of Zhou et al. (2022) and Brandenburg et al. (2023), who considered different values of Lu and also included some runs with hyperviscosity and hyperresistivity, unlike what we present in the present work. At variance with those earlier papers, where the focus was always on the decay exponent $p(t)$, here we focus on the evolution of the decay time, $\tau(t) = t/p(t)$.

4.1. Decay time

The goal is to determine the prefactor in the scaling relation $\tau \propto \xi_M/v_A$. Therefore, we write

$$t/p \equiv \tau = C_M \xi_M / v_A \tag{10}$$

and determine

$$C_M(t) = (t/p)\, v_A(t)/\xi_M(t). \tag{11}$$

We emphasize here that each of the terms is time-dependent, including $\tau(t) = t/p(t)$, as already stressed above. Interestingly, it turns out that the quantity $C_M(t)$ eventually settles around a plateau,

$$C_M = \lim_{t\to\infty} C_M(t). \tag{12}$$

Here and in the following, when time-dependence is not indicated, we usually mean that the value is obtained as a suitable limit of the corresponding time-dependent function. Of course, in numerical simulations with finite domains, the limit $t \to \infty$ needs to be evaluated with some care so as to avoid that the final result is contaminated by finite size effects. We do this by selecting a suitable time interval during which certain data combinations are approximately statistically stationary. We refer to those results as late-time limits.

In Fig. 4 we show that $C_M(t)$ and $\mathrm{Lu}(t)$ approach an approximately constant value towards the end of the run. Time is given both in unit of $[t] = (c_s k_1)^{-1}$ and in initial Alfvén times, $(v_{A0}k_p)^{-1}$, where $v_{A0} = \sqrt{2\mathcal{E}_{M0}}$ is the initial Alfvén velocity and $\mathcal{E}_{M0}$ the initial magnetic energy density. Allowing for the possibility of power-law scaling, $C_M = C_L^{(n)}\mathrm{Lu}^n$, we also plot the prefactor $C_L^{(n)}(t)$ for $n = 1/4$ in the last panel of Fig. 4; see details below. Towards the end of the simulation, however, there is an increase in the fluctuations, which follows from the decrease in the magnetic energy.

As discussed later in more detail in connection with 2–D simulations, current sheets are underresolved at early times, when ξ_M is small. As we now see from Fig. 4, this underestimates the resulting value of C_M. However, for $t > 100$, $C_M(t)$ approaches a plateau, suggesting that the simulation now begins to be sufficiently well resolved – at least for the purpose of determining C_M.

In Fig. 5, we show the dependence of C_M on Lu and Lu_ν. We see an approximate scaling $\propto \mathrm{Lu}^n$ with $n = 1/4$ for $\mathrm{Lu} < 6000$ and a piecewise power-law scaling $\propto \mathrm{Lu}_\nu^{1/2}$, but with different prefactors for the runs with larger and smaller values of the viscosity. Note that for $\mathrm{Pr_M} \gg 1$, we have $\mathrm{Lu}_\nu = v_A \xi_M/\sqrt{\eta\nu}$, which explains why the $\mathrm{Lu}_\nu^{1/2}$ scaling is found to be compatible with being $\propto \mathrm{Lu}^{1/4}$. Note, however, that for a larger viscosity, the line $\mathrm{Lu}_\nu^{1/2}$ is shifted upwards (towards larger values of C_M). Owing to the more complicated combined dependence on ν and Lu_ν, we con-

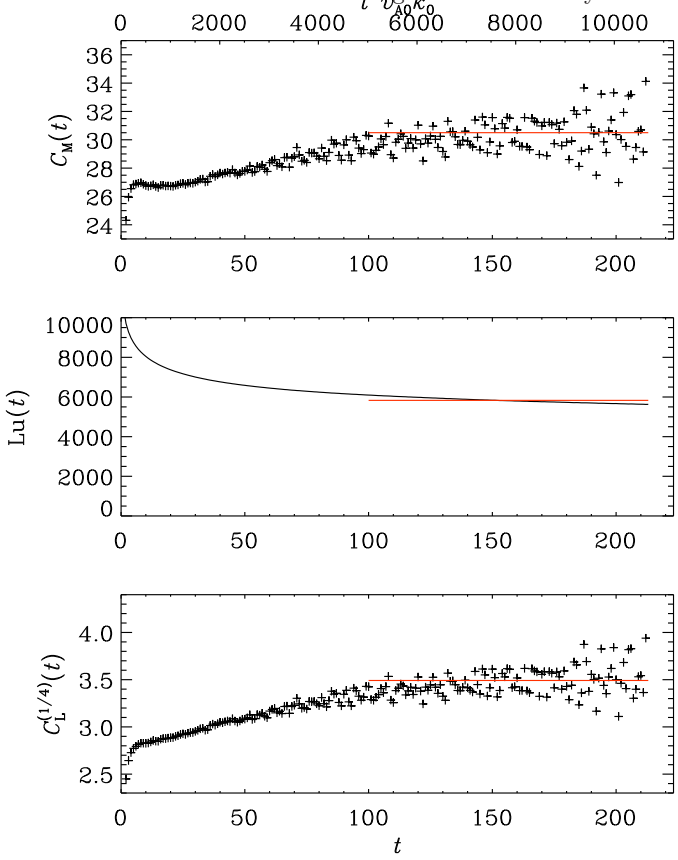

Fig. 4. Approach of $C_{\rm M}(t)$, Lu(t), and $C_{\rm L}^{(1/4)}(t)$ to an approximately constant value toward the end of the simulation for Run M1.

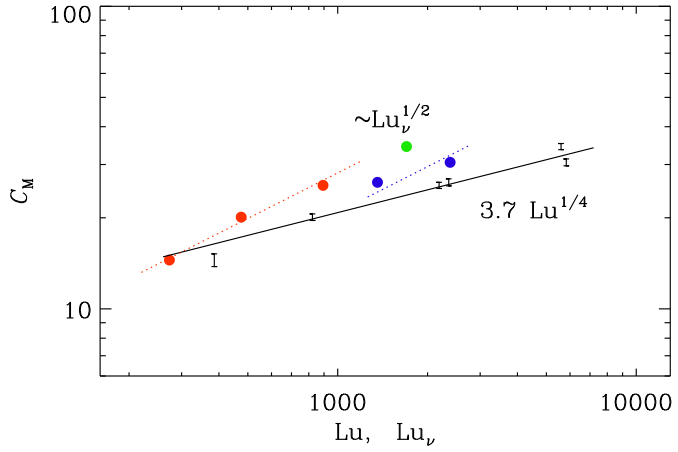

Fig. 5. Dependence of $C_{\rm M}$ on Lu and Lu$_\nu$. Note the approximate scaling $\propto {\rm Lu}^{1/4}$ for Lu < 6000 and a piecewise power-law scaling $\propto {\rm Lu}_\nu^{1/2}$ with different prefactors for the runs with larger viscosity (5×10^{-6} red symbols and 4×10^{-6} for the green symbol) and smaller viscosity (2×10^{-6} blue symbols).

tinue to employ the simpler Lu^n scaling for the following discussion. It is worth noting that the exponent $n=1/4$ has been discussed by Uzdensky & Loureiro (2016) in connection with the fast growing mode of the tearing instability.

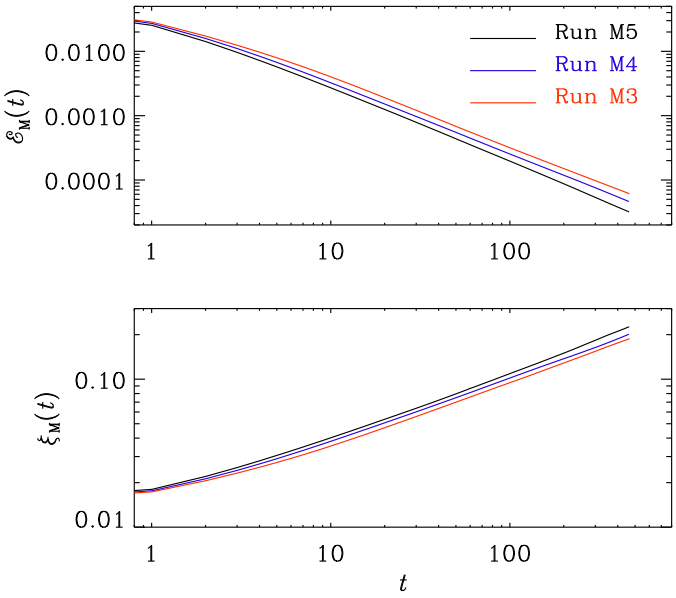

Fig. 6. Dependence of $\mathcal{E}_{\rm M}(t)$ and $\xi_{\rm M}(t)$ for three values of ${\rm Pr}_{\rm M}$.

If it is really true that $C_{\rm M}$ is proportional to Lu^n, as found above, we can write $C_{\rm M}=C_{\rm L}^{(n)}{\rm Lu}^n$, and then determine $C_{\rm L}^{(n)}$ as the late-time limit of

$$C_{\rm L}^{(n)}(t)=\frac{t}{p}\,\frac{v_{\rm A}^{1-n}}{\xi_{\rm M}^{1+n}}\,\eta^n. \tag{13}$$

This is the formula that was used to compute $C_{\rm L}^{(n)}$ and to plot its time-dependence $C_{\rm L}^{(n)}(t)$ for $n=1/4$; see the last panel of Fig. 4. Looking at Table 1, we find $3.3\le C_{\rm L}^{(1/4)}\le 3.8$.

4.2. Evolution of $\mathcal{E}_{\rm M}(t)$ and $\xi_{\rm M}(t)$

It is of interest to know whether the resistivity dependence of $C_{\rm M}(t)$ is equally distributed among $\xi_{\rm M}$ and $v_{\rm A}$ (or $\mathcal{E}_{\rm M}$). Figure 6 shows that there are indeed systematic differences in the decay laws for different values of the resistivity, but the differences are small and easily overlooked.

To examine the dependence of $C_{\rm M}(t)$ on Lu, we write the decay laws for $\xi_{\rm M}(t)$ and $\mathcal{E}_{\rm M}(t)$ in a more detailed form than Eq. (1), i.e.,

$$\xi_{\rm M}(t)=\xi_{\rm M0}\,(1+t/\tau_\xi)^q, \tag{14}$$

$$\mathcal{E}_{\rm M}(t)=\mathcal{E}_{\rm M0}\,(1+t/\tau_\mathcal{E})^{-p}. \tag{15}$$

Here, the coefficients $\xi_{\rm M0}$ and $\mathcal{E}_{\rm M0}$ just depend on the initial condition and are thus not dependent on Lu, so the Lu-dependence can only enter through the coefficients τ_ξ and $\tau_\mathcal{E}$. We can determine them as the limits of the time-dependent functions $\tau_\xi(t)$ and $\tau_\mathcal{E}(t)$, which are obtained by inverting Eqs. (14) and (15), and are given by

$$\tau_\xi(t)=\frac{t}{[\xi_{\rm M}(t)/\xi_{\rm M0}]^{1/q}-1}, \tag{16}$$

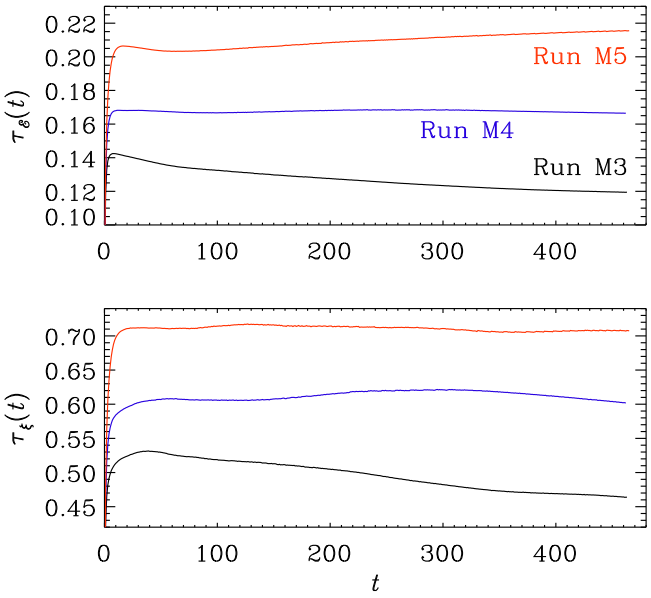

Fig. 7. Evolution of $\tau_\mathcal{E}(t)$ and $\tau_\xi(t)$ for three values of $\mathrm{Pr_M}$ with fixed and moderate viscosity. Note that these times tend to be approximately constant a late times with values approximately consistent with those in Table 1.

$$\tau_\mathcal{E}(t) = \frac{t}{[\mathcal{E}_\mathrm{M}(t)/\mathcal{E}_\mathrm{M0}]^{-1/p} - 1}. \tag{17}$$

Figure 7 shows the evolution of $\tau_\xi(t)$ and $\tau_\mathcal{E}(t)$ for Runs M3–M5 with fixed and moderate viscosity.

Using the late-time limits of Eqs. (14) and (15), as well as those of Eqs. (16) and (17), the equation for C_M can now be decomposed in the form

$$C_\mathrm{M} = C_\xi C_\mathcal{E}, \tag{18}$$

such that Eq. (11) is obeyed. Here, we can determine C_ξ and $C_\mathcal{E}$ as the late-time limits of

$$C_\xi(t) = \tau^q \xi_\mathrm{M}^{-1} \quad \text{and} \quad C_\mathcal{E}(t) = \tau^{p/2} v_\mathrm{A}. \tag{19}$$

In this connection, it it important to remember that for a self-similar evolution (Brandenburg & Kahniashvili 2017), which is here approximately satisfied (see Fig. 3), we have

$$q + p/2 = 1, \tag{20}$$

so that $C_\mathrm{M} = (t/p)\, v_\mathrm{A}/\xi_\mathrm{M}$ is obeyed. For $t \gg \tau_\mathcal{E}, \tau_\xi$, using again $\tau = \tau(t) = t/p(t)$, we have

$$C_\xi \approx (\tau_\xi/p)^q \xi_\mathrm{M0}^{-1} \quad \text{and} \quad C_\mathcal{E} \approx (\tau_\mathcal{E}/p)^{p/2} v_\mathrm{A0}. \tag{21}$$

so that $C_\mathrm{M} = (v_\mathrm{A0}/p\xi_\mathrm{M0})\, \tau_\xi^q \tau_\mathcal{E}^{p/2}$. It is then natural to expect that both τ_ξ and $\tau_\mathcal{E}$ scale in the same way with Lu as C_M itself. Equation (21) also allows us to compute the timescales $\tau_\xi = p\,(C_\xi \xi_\mathrm{M0})^{1/q}$ and $\tau_\mathcal{E} = p\,(C_\mathcal{E}/v_\mathrm{A0})^{2/p}$.

In Fig. 8, we show the dependence of τ_ξ and $\tau_\mathcal{E}$ on Lu. Note that, while the two show a similar dependence approximately $\propto \mathrm{Lu}^{1/4}$, there possibly is also evidence for a leveling off for larger values of Lu.

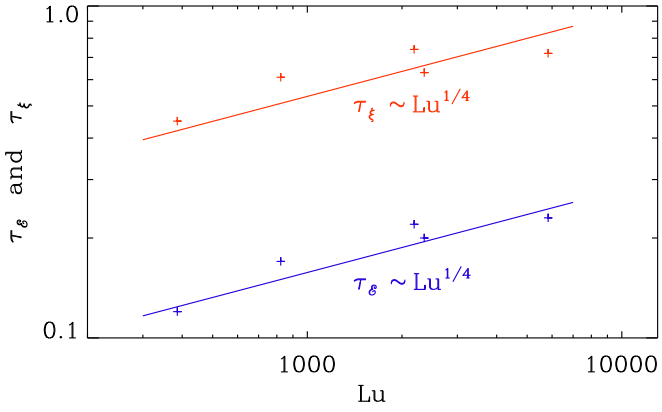

Fig. 8. Dependence of τ_ξ and $\tau_\mathcal{E}$ on Lu. The two show a similar dependence on Lu approximately $\propto \mathrm{Lu}^{1/4}$, but there is possibly also evidence for a leveling off for larger values of Lu.

5. Comparison with hydrodynamic decay

Hydrodynamic decay is characterized by the kinetic energy density $\mathcal{E}_\mathrm{K}(t) = \rho_0 u_\mathrm{rms}^2/2$ and the hydrodynamic integral scale $\xi_\mathrm{K}(t) = \int k^{-1} E_\mathrm{K}\, \mathrm{d}k/\mathcal{E}_\mathrm{K}$. We define the instantaneous kinetic energy decay exponent $p_\mathrm{K}(t) = -\mathrm{d}\ln\mathcal{E}_\mathrm{K}/\mathrm{d}\ln t$ and the decay time $\tau_\mathrm{K}(t) = t/p_\mathrm{K}(t)$. We relate $\tau_\mathrm{K}(t)$ to the turnover time $u_\mathrm{rms}/\xi_\mathrm{K}$ through $\tau_\mathrm{K} = C_\mathrm{K}\xi_\mathrm{K}/u_\mathrm{rms}$, and thus determine C_K as the late-time limit of $C_\mathrm{K}(t) = [t/p_\mathrm{K}(t)]\, u_\mathrm{rms}(t)/\xi_\mathrm{K}(t)$, which is defined analogously to Eq. (11).

Purely hydrodynamic simulations can be performed by just ignoring the magnetic field, or putting $\boldsymbol{B} = 0$. In Table 2, we summarize such simulations for different values of ν, which is quantified by the Reynolds number, $\mathrm{Re} = u_\mathrm{rms}\xi_\mathrm{K}/\nu$. Figure 9 shows that, for $\mathrm{Re} \geq 100$, C_K does not change much with Re. This was also not expected. It also confirms that the prolonged decay time found in Sect. 4 is indeed a purely magnetic phenomenon. Whether or not the resistivity dependence in the magnetic case must be ascribed to reconnection remains an open question. As discussed in Sect. 2, magnetic reconnection refers to topologically constrained changes of magnetic field lines, but in the present case of a turbulent magnetic field, there is no connection with the standard picture of reconnection. An obvious alternative candidate for explaining the resistively prolonged decay time may be related to magnetic helicity conservation in local patches, as described by the conservation of the Hosking integral. While this idea seems more plausible to us, it is not obvious how to distinguish reconnection from magnetic helicity conservation in patches. It is true that magnetic helicity would vanish in two dimensions, but in that case it should be replaced by the anastrophy; see Appendix A for a historical note on this word. One aspect that might be different between the concepts of reconnection and magnetic helicity conservation in patches could be the dependence on $\mathrm{Pr_M}$. Our present results have not yet shown such a dependence, which might support the idea that the dependence on resistivity is related to magnetic helicity conservation in patches.

Table 2. Summary of hydrodynamic simulations discussed in Sect. 5.

Run	$\nu k_1/c_s$	Re	C_K	$C_L^{(1/4)}$	C_ξ	$C_\mathcal{E}$	τ_ξ	$\tau_\mathcal{E}$	N^3
H1	1×10^{-7}	573	5.5 ± 0.5	1.1	230	0.024	7.5	0.12	1024^3
H2	2×10^{-7}	280	5.8 ± 1.0	1.4	234	0.024	7.8	0.12	1024^3
H3	5×10^{-7}	134	4.9 ± 0.5	1.4	205	0.024	5.8	0.12	1024^3
H4	1×10^{-6}	110	4.4 ± 0.6	1.4	164	0.027	3.5	0.16	1024^3
H5	2×10^{-6}	35	3.7 ± 0.7	1.5	167	0.022	4.9	0.13	512^3

Table 3. Similar to Table 1, but for the two-dimensional hydromagnetic simulations analyzed in Sect. 6. Here, $k_p/k_1 = 200$.

Run	$\eta k_1/c_s$	$\nu k_1/c_s$	$\mathrm{Pr_M}$	Lu	C_M	$C_L^{(1/4)}$	C_ξ	$C_\mathcal{E}$	τ_ξ	$\tau_\mathcal{E}$	ϵ_K/ϵ_M	$\mathrm{Ma_A}$	N^2
2m1	5×10^{-9}	5×10^{-7}	100	75,000	36.7 ± 4.6	2.2	221	0.164	0.34	1.26	13	0.41	16384^2
2m2	2×10^{-9}	2×10^{-7}	100	182,000	39.5 ± 1.0	1.9	241	0.164	0.41	1.25	21	0.43	16384^2
2m3	1×10^{-9}	1×10^{-7}	100	358,000	42.7 ± 1.7	1.7	254	0.168	0.46	1.30	33	0.44	16384^2
2m4	1×10^{-9}	2×10^{-8}	20	356,000	43.8 ± 2.5	1.8	248	0.175	0.50	1.50	11	0.44	8192^2
2m5	2×10^{-9}	2×10^{-8}	10	178,000	43.9 ± 3.0	2.1	247	0.177	0.49	1.53	6.0	0.44	8192^2
2m6	2×10^{-9}	2×10^{-8}	10	178,000	45.3 ± 1.8	2.2	254	0.178	0.47	1.45	6.0	0.44	16384^2
2M1	4×10^{-9}	2×10^{-8}	5	90,800	42.5 ± 2.1	2.4	241	0.175	0.47	1.34	3.5	0.45	8192^2
2M2	2×10^{-8}	1×10^{-7}	5	19,000	36.8 ± 2.6	3.1	217	0.169	0.37	1.40	2.9	0.45	8192^2
2M3	1×10^{-7}	5×10^{-7}	5	3900	30.2 ± 2.0	3.8	191	0.157	0.34	1.36	1.5	0.42	4096^2
2M4	1×10^{-7}	5×10^{-7}	5	770	18.9 ± 0.6	3.6	347	0.054	1.30	3.66	0.8	0.42	4096^2
2M5	1×10^{-9}	1×10^{-9}	1	365,000	44.1 ± 1.8	1.8	252	0.175	0.52	1.49	0.7	0.44	8192^2
2M6	5×10^{-9}	5×10^{-9}	1	72,300	39.9 ± 1.9	2.4	232	0.171	0.43	1.43	0.8	0.46	8192^2
2M7	2×10^{-8}	2×10^{-8}	1	18,700	36.8 ± 1.7	3.1	233	0.157	0.44	1.23	0.8	0.46	8192^2
2M8	1×10^{-7}	1×10^{-7}	1	3830	31.0 ± 0.7	3.9	213	0.146	0.35	1.07	0.7	0.45	8192^2
2M9	5×10^{-7}	5×10^{-7}	1	742	18.7 ± 0.8	3.6	156	0.119	0.22	0.83	0.5	0.51	4096^2
2M10	5×10^{-7}	5×10^{-7}	1	125	10.0 ± 0.4	3.0	284	0.035	0.83	1.66	0.5	0.63	4096^2

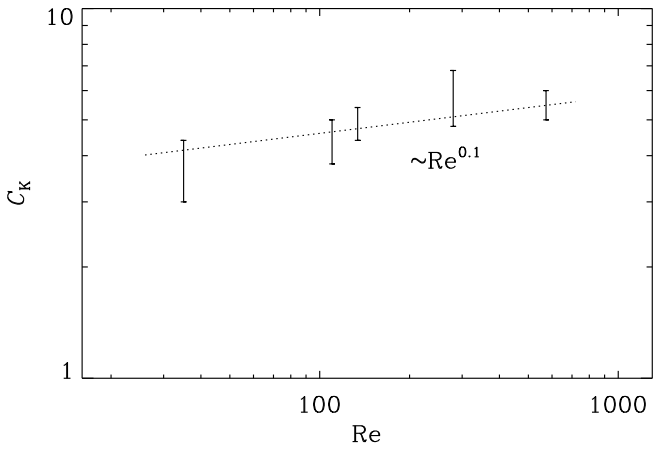

Fig. 9. Dependence of C_K on Re. The line $\mathrm{Re}^{0.1}$ is shown for comparison, but the data are also nearly compatible with being independent of Re.

6. Hydromagnetic decay in two dimensions

We now perform 2–D simulations where $\boldsymbol{B} = \boldsymbol{\nabla}\times(\hat{\boldsymbol{z}}A_z)$ lies entirely in the xy plane; see Table 3 for a summary. Equation (7) then reduces to

$$\frac{\mathrm{D}A_z}{\mathrm{D}t} = \eta\nabla^2 A_z, \tag{22}$$

which obeys conservation of anastrophy, $\langle A_z^2\rangle = \mathrm{const}$ (Fyfe & Montgomery 1976; Pouquet 1978, 1993), and the magnetic helicity density vanishes pointwise, so the Hosking integral is then also zero. These simulations are different from recent ones by Dwivedi et al. (2024), who performed 2.5–D simulations. In their case, there was a magnetic field component out of the plane. The anastrophy was then not conserved and the Hosking integral was finite.

As we stated above, our present measurements of C_M as a function of Lu cannot directly be compared with the reconnection rate determined by Loureiro et al. (2012), Comisso et al. (2015), or Comisso & Bhattacharjee (2016). In addition, it is not obvious how relevant a 2–D simulation is in the present context, because in 2–D, the anastrophy is conserved, while the Hosking integral is strictly vanishing.

In our present purely 2–D simulations, values of Lu up to about 3×10^5 have been reached. To allow for a longer nearly selfsimilar evolution, we have used $k_p/k_1 = 200$ instead of 60. The simulation results give the prefactors in the scaling expected from anastrophy conservation as

$$\xi_M(t) \approx 0.13\,\langle A_z^2\rangle^{1/4}\,t^{1/2}, \quad \mathcal{E}_M(t) \approx 15\,\langle A_z^2\rangle^{1/2}\,t^{-1}, \tag{23}$$

where $\mu_0 = \rho_0 = 1$ has been used. We also see from Fig. 10 that the spectral peaks evolve underneath an envelope $E_M(k,t) \le 60\,\langle A_z^2\rangle\,k$.

Figure 11 shows magnetic and kinetic energy spectra for Run 2m2 with $\mathrm{Lu} = 1.8\times10^5$ collapsed on top of each other by plotting $\xi_M^\beta(t)E_M\big(k\xi_M(t)\big)$ versus $k\xi_M(t)$ for $\beta = 1$. This plot suggests that the subinertial range scalings of $E_M(k,t)$

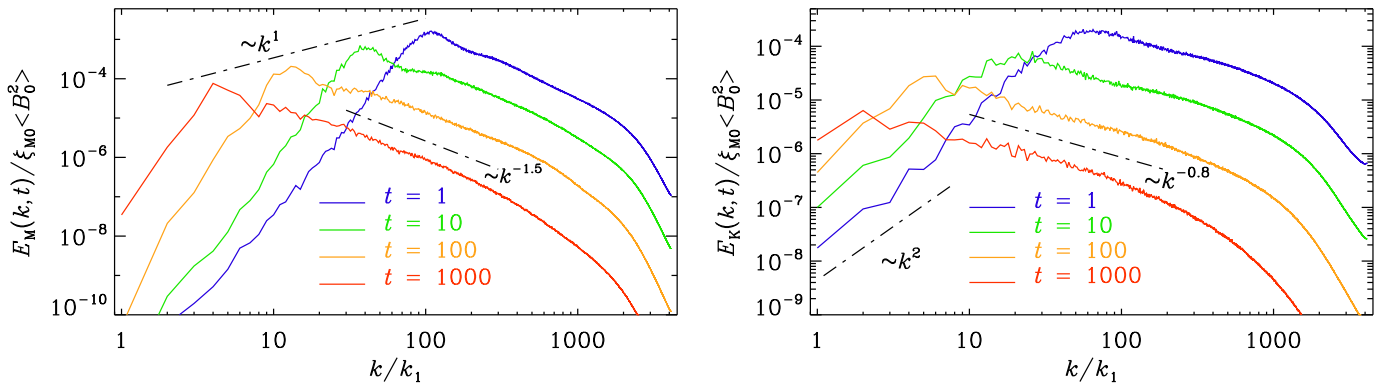

Fig. 10. Similar to Fig. 3, but for Run 2M1. Note that the magnetic peaks lie underneath a k^β envelope with $\beta = 1$, as expected in the case of anastrophy conservation.

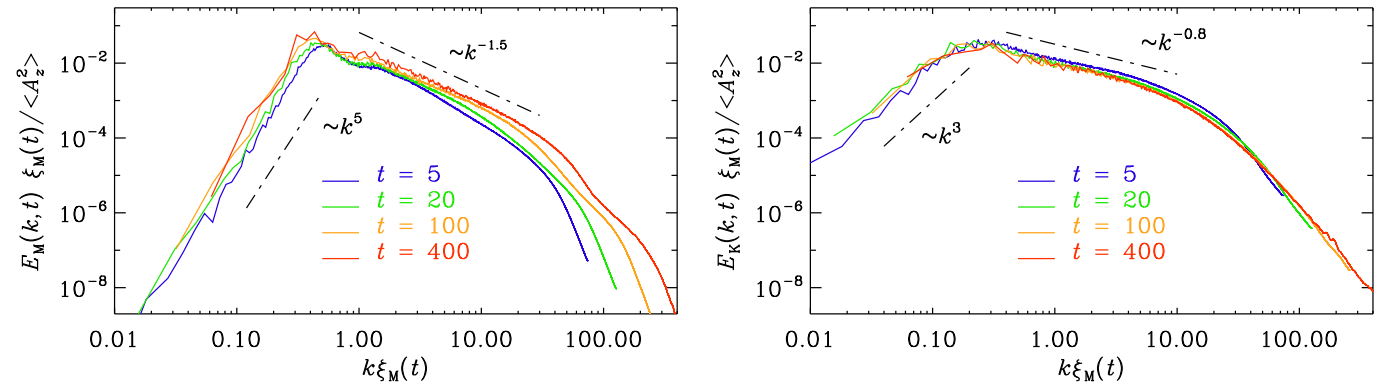

Fig. 11. Magnetic energy spectra (left) and kinetic energy spectra (right) for Run 2m2 with $\mathrm{Lu} = 1.8 \times 10^5$ and $\mathrm{Pr_M} = 100$, at times $t = 5$, 20, 100, and 400, collapsed on top of each other by plotting both versus $k\xi_M(t)$ and scaling them with ξ_M. This makes their heights agree, as expected.

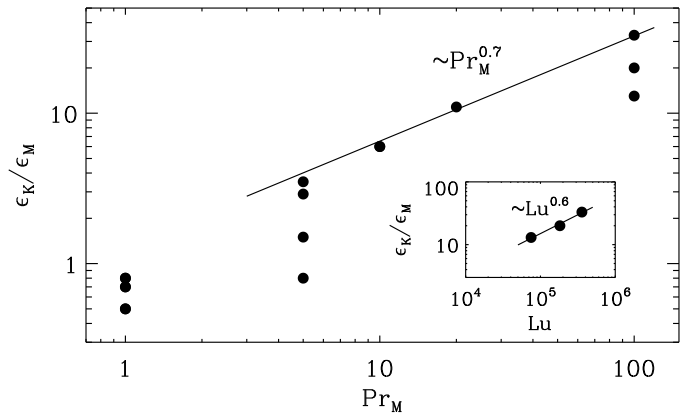

Fig. 12. Dependence of ϵ_K/ϵ_M on $\mathrm{Pr_M}$. The solid line denotes $1.3\,\mathrm{Pr_M^{0.7}}$, but many of the data points, predominantly those with smaller Lu, are beneath that line. The inset shows that for $\mathrm{Pr_M} = 100$, ϵ_K/ϵ_M increases with Lu like $\mathrm{Lu}^{0.6}$.

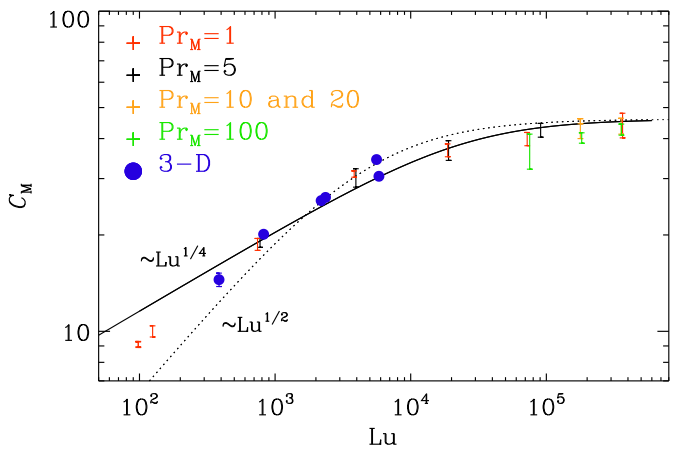

Fig. 13. Dependence of C_M on Lu for the 2–D runs. Note the shallow scaling $\propto \mathrm{Lu}^{0.1}$ for $10^4 < \mathrm{Lu} < 10^5$, which is also compatible with a leveling off at $\mathrm{Lu_c} = 2.5 \times 10^4$, as described by Eq. (24) with $n = 1/4$. The black (red) data points are for $\mathrm{Pr_M} = 5$ ($\mathrm{Pr_M} = 1$). The blue data points denote the 3–D results from Sect. 4. The orange symbols are for the runs with $\mathrm{Pr_M} = 10$ and 20, listed in Table 3. The thin dotted line gives Eq. (24) with $n = 1/4$ for comparison.

and $E_K(k,t)$ are proportional to k^5 and k^3, respectively. Thus, they are steeper than expected in 3-D. This behavior is in some ways similar to the steepening observed for helical

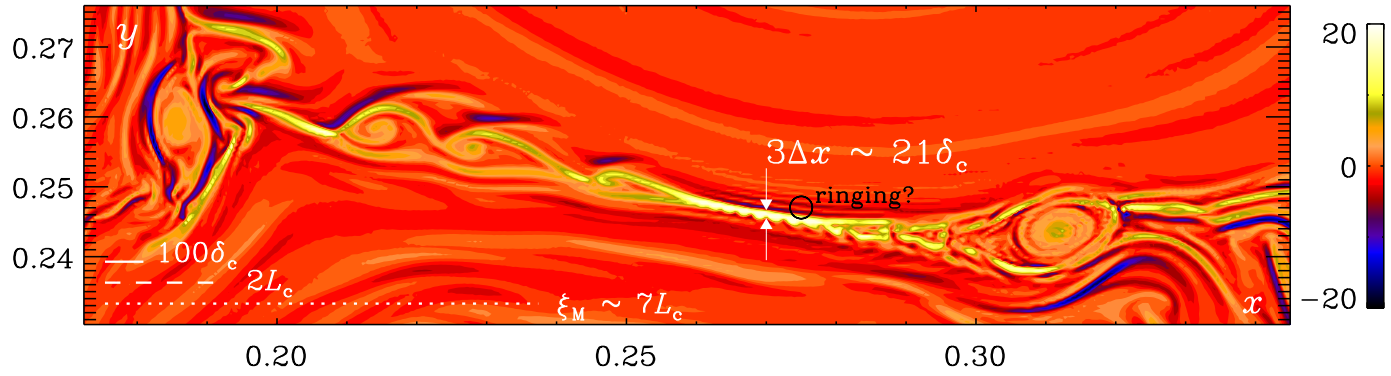

Fig. 14. Visualization of $J_z(x,y)$ of Run 2m6 with $\mathrm{Pr_M}=10$, $\mathrm{Lu}=1.8\times10^5$, $\mathrm{Lu}_\nu\approx5\times10^4$, and 16384^2 mesh points at $t=464$ for a small part of the domain with sizes $2.8\xi_\mathrm{M}(t)\times0.74\xi_\mathrm{M}(t)$. The lengths of $100\,\delta_\mathrm{c}$, $2L_\mathrm{c}$, and ξ_M are indicated by horizontal white solid, dashed, and dotted lines, respectively. The thickness of the current sheet corresponds to about $3\Delta x\approx21\,\delta_\mathrm{c}$. In its proximity, there are also indications of ringing, indicated by the black circle.

decaying magnetic fields; see Brandenburg & Kahniashvili (2017).

In Table 3, we also give the ratio $\epsilon_\mathrm{K}/\epsilon_\mathrm{M}$, which is seen to increase with $\mathrm{Pr_M}$; see Fig. 12. This was expected based on earlier results (Brandenburg 2014; Galishnikova et al. 2022), but it was never shown in the decaying case of magnetically dominated turbulence. We see that $\epsilon_\mathrm{K}/\epsilon_\mathrm{M}\propto\mathrm{Pr_M^{0.7}}$, which is similar to the previously studied case with large-scale dynamo action rather than the case with just small-scale action, where the slope was shallower. The ratio $\epsilon_\mathrm{K}/\epsilon_\mathrm{M}$ is found to increase also with Lu, at least for $\mathrm{Lu}\ll10^6$. As discussed in Brandenburg & Rempel (2019), an increase of $\epsilon_\mathrm{K}/\epsilon_\mathrm{M}$ with $\mathrm{Pr_M}$ may have implications for heating the solar corona, where the possible dominance of kinetic energy dissipation over Joule dissipation is not generally appreciated; see Rappazzo et al. (2007, 2018) for earlier work discussing this ratio.

Although 2–D and 3–D runs are in many ways rather different from each other, we now determine the same diagnostics as in the 3–D case; see Table 3 and Fig. 13 for a plot of C_M versus Lu. We see that the C_M dependence on Lu is qualitatively similar for 2–D and 3–D turbulence. Moreover, it becomes shallower for larger values of Lu. There is now evidence for C_M to level off and to become independent of Lu. It is possible to fit our data to a function of the form

$$C_\mathrm{M}(\mathrm{Lu})\approx C_\mathrm{L}^{(1/4)}\left(\frac{\mathrm{Lu}}{1+\mathrm{Lu}/\mathrm{Lu_c}}\right)^n, \tag{24}$$

where $\mathrm{Lu_c}=2.5\times10^4$ is a critical Lundquist number characterizing the point where the dependence levels off, $n=1/4$, and $C_\mathrm{L}^{(1/4)}=3.7$. The value of $\mathrm{Lu_c}$ is larger than that found by Loureiro et al. (2012), where the asymptotes for small and large Lundquist numbers cross at a value closer to 5000. However, this difference could simply be related to different definitions of the relevant length scales. (Note that our definition of ξ_M does not include a 2π factor.) A comparison with the Sweet-Parker value of $n=1/2$ results in reasonable agreement for small values of Lu, but there are rather noticeable departures from the data for intermediate values.

Our 2–D and 3–D results for C_M are seen to be in good agreement with each other, which is similar to the observation made by Bhat et al. (2021). Obviously, larger simulations should still be performed to see whether the agreement between 2–D and 3–D continues to larger Lundquist numbers.

It should also be noted that some of our data with their nominal error bars do not lie on the fit given by Eq. (24) with $n=1/4$. Especially for $\mathrm{Pr_M}=100$ and smaller values of Lu, we see that C_M lies systematically below the fit. It shall be noted, however, that one would have expected an increase with $\mathrm{Pr_M}$ like $(1+\mathrm{Pr_M})^{1/2}$, i.e., the opposite trend, if the reconnection phenomenology was applicable; see Eq. (16) of Hosking & Schekochihin (2023).

To check whether our simulations are sufficiently well resolved, we show in Fig. 14 a visualization of $J_z(x,y)$ for Run 2m6 with $\mathrm{Pr_M}=10$ and 16384^2 mesh points at $t=464$ for a small part of the domain with sizes $2.8\xi_\mathrm{M}(t)\times0.74\xi_\mathrm{M}(t)$ where a large current sheet breaks up into smaller plasmoids. A comparison between Runs 2m5 and 2m6 with 8192^2 and 16384^2 mesh points is shown in Appendix B. Our main conclusions are that higher resolution suppresses the tendency to produce ringing, i.e., the formation of oscillations on the grid scale, but that the results for C_M are not very sensitive to the numerical resolutions, as can be seen by comparing Runs 2m5 and 2m6 in Table 3.

Next, we compare the typical length and thickness of current sheets in Run 2m6 with the values defined by Uzdensky et al. (2010) for critical current sheets, $L_\mathrm{c}=\mathrm{Lu_c}\,\eta/v_\mathrm{A}$ and $\delta_\mathrm{c}=L_\mathrm{c}/\mathrm{Lu_c^{1/2}}$, respectively. These lengths are indicated in Fig. 14. Here, we used $\mathrm{Lu_c}=2.5\times10^4$ as the critical Lundquist number, which was found to be representative of all of our cases. We see that the current sheets in Fig. 14 have a length that is comparable to $\xi_\mathrm{M}\approx7\,L_\mathrm{c}$. This is just because $\mathrm{Lu}\approx7\,\mathrm{Lu_c}$. The thickness of the current sheets is about $20\,\delta_\mathrm{c}$. They are marginally resolved with about $3\Delta x$, where $\Delta x=2\pi/16384\approx3.8\times10^{-4}$ is the mesh spacing. Thus, the aspect ratio of thickness to length of the current sheets is about $20\,\delta_\mathrm{c}/7\,L_\mathrm{c}=(20/7)\,\mathrm{Lu_c^{-1/2}}\approx0.02$. This is about three times the nominal value estimated by Uzdensky et al. (2010) for critical current sheets.

By comparison, Hosking & Schekochihin (2023) estimated for the aspect ratio $\delta_\mathrm{c}/\xi_\mathrm{M}=\mathrm{Lu_c^{1/2}}/\mathrm{Lu}_\nu$. For Run 2m6 with $\mathrm{Lu}_\nu\approx5\times10^4$, this yields 0.003, which is about six times smaller than our value of 0.02. While

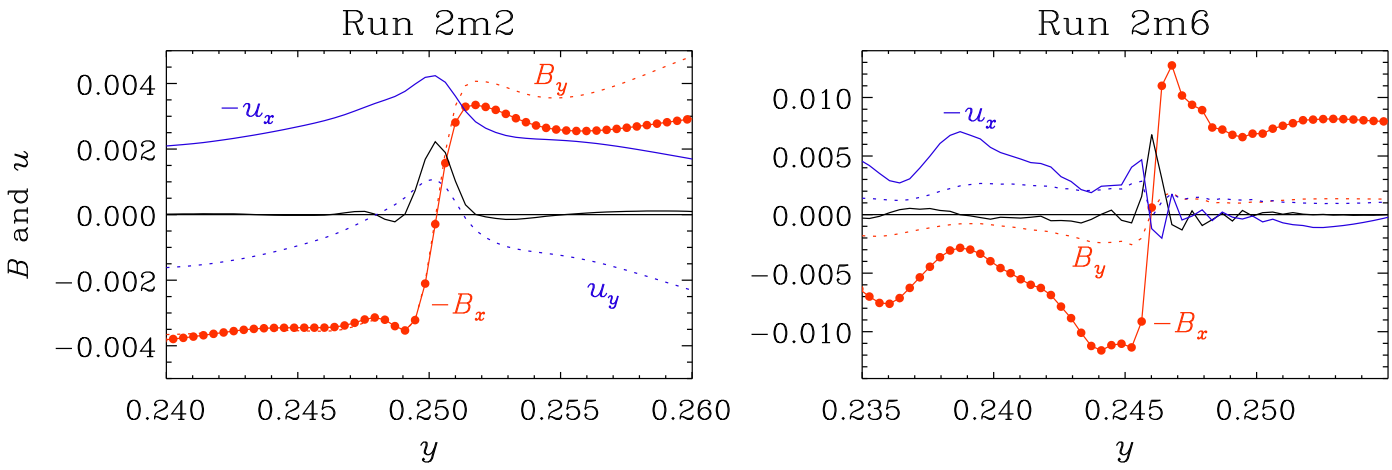

Fig. 15. Magnetic field profiles [$-B_x(y)$ and $B_y(y)$ in red] and velocity profiles [$-u_x(y)$ and $u_y(y)$ in blue] through the current sheet (in black) for Run 2m2 (through $x = 0.372$) and Run 2m6 (through $x = 0.270$).

these discrepancies could perhaps be explained by the absence of nondimensional prefactors in the definitions of δ_c, we must also consider the possibility that this is simply a consequence of a lack of resolution.

Runs 2m2 and 2m6 have in common that they have the same resistivity and nearly the same value of Lu of about 1.8×10^5, but Run 2m2 has a tenfold larger viscosity than Run 2m6, so $\mathrm{Pr_M}$ is increased from 10 to 100. We see that C_M has deceased by only about 15%, which is much less than what is expected if C_M was proportional to $\mathrm{Pr_M^{-1/2}}$.

In Fig. 15, we show for Runs 2m2 and 2m6 magnetic field profiles, $-B_x(y)$ and $B_y(y)$, and velocity profiles, $-u_x(y)$ and $u_y(y)$, through a particular current sheet. We see that in Run 2m2 with $\mathrm{Pr_M} = 100$, the profiles are much smoother, even though the value of $\mathrm{Lu} = 1.8 \times 10^5$ is the same in both cases. Thus, the viscosity has a significant effect in smoothing the magnetic field. Yet, the effect on the value of C_M is small.

7. Endpoints in the primordial evolutionary diagram

The evolution of primordial magnetic fields is usually displayed in an evolutionary diagram showing the comoving values of B_rms versus ξ_M, or, what is similar, v_A versus ξ_M. This dependence corresponds to a power law of the form $v_\mathrm{A} = v_\mathrm{A0}(\xi_\mathrm{M}/\xi_\mathrm{M0})^\kappa$. Since $\xi_\mathrm{M}(t) \sim t^q$, we have $v_\mathrm{A}(t) \sim t^{-p/2} \sim \xi_\mathrm{M}^{-p/2q}$, so $\kappa = p/2q = 5/4$ for the Hosking scaling with $p = 10/9$ and $q = 4/9$.

Following Banerjee & Jedamzik (2004), the time t in Eq. (10) would be replaced by the age of the Universe at the time of recombination, t_rec. As emphasized by Hosking & Schekochihin (2023), this gives an implicit equation for the magnetic field at recombination with the solution $B(t_\mathrm{rec}) \approx 10^{-8.5}\,\mathrm{G}\,(\xi_\mathrm{M}/1\,\mathrm{Mpc}) = 10^{-14.5}\,\mathrm{G}\,(\xi_\mathrm{M}/1\,\mathrm{pc})$ if $C_\mathrm{M} = 1$. However, $B(t_\mathrm{rec})$ would be much larger and ξ_M much smaller when $C_\mathrm{M} \gg 1$ is taken into account.

Under the hypothesis of fast reconnection owing to plasmoid instability (Bhattacharjee et al. 2009; Uzdensky et al. 2010), Hosking & Schekochihin (2023) estimated C_M as the square root of some effective cutoff value of about 10^4 for the Lundquist number and an additional factor of $\mathrm{Pr_M^{1/2}}$. Here, they estimated $\mathrm{Pr_M} \approx 10^7$, so $C_\mathrm{M} = 10^{5.5}$ and $B(t_\mathrm{rec}) \approx 10^{-3}\,\mathrm{G}\,(\xi_\mathrm{M}/1\,\mathrm{Mpc}) = 10^{-9}\,\mathrm{G}\,(\xi_\mathrm{M}/1\,\mathrm{pc})$.

Our new results challenge the reliability of the anticipated dependence of C_M on $\mathrm{Pr_M}$. With the current results at hand, Fig. 13 suggests that C_M never exceeds the value $3.7\,\mathrm{Lu_c^{1/4}} \approx 47$, even for $\mathrm{Pr_M}$ as large as 100. Particularly important is the fact that this result is independent of $\mathrm{Pr_M}$. Given that Hosking & Schekochihin (2023) used $\mathrm{Pr_M} \approx 10^7$, which yielded an extra $10^{3.5}$ factor and therefore $C_\mathrm{M} = 10^{5.5}$ in their estimate, our new findings imply that the resistivity effect is actually independent of $\mathrm{Pr_M}$. Although this has so far only been verified for values of $\mathrm{Pr_M} \leq 5$, we suggest that a more accurate formula for the endpoints of the evolution with $C_\mathrm{M} = 47 \approx 10^{1.7}$ would be $B(t_\mathrm{rec}) \approx 10^{-6.8}\,\mathrm{G}\,(\xi_\mathrm{M}/1\,\mathrm{Mpc}) = 10^{-12.8}\,\mathrm{G}\,(\xi_\mathrm{M}/1\,\mathrm{pc})$. These values are still above the lower limits inferred from suppressed GeV photon emission from the halos of blazars (Neronov & Vovk 2010).

8. Conclusions

The present results have shown that, up to the largest Lundquist numbers accessible to our present direct numerical simulations with 2048^3 mesh points, the decay times depend on the resistivity. Only for our 2–D simulations do we see evidence for a cutoff. The dependence of hydromagnetic turbulence properties on the value of the resistivity is unusual for fully developed turbulence. One wonders whether our results reflect just a peculiar property of decaying turbulence, or whether there could also exist aspects of statistically stationary turbulence that depend on the microphysical resistivity. Possible examples of resistively controlled time dependencies could include the time that is needed to develop the final saturated magnetic energy spectrum in kinetically forced turbulence, where the magnetic field emerges due to a dynamo action (Haugen et al. 2003; Schekochihin et al. 2004). A resistively slow adjustment phase is reminiscent of what occurs for helical magnetic fields (Brandenburg 2001), where it has also been possible to measure a weak resistivity dependence of the turbulent magnetic diffusivity (Brandenburg et al. 2008).

In the present 3–D case, of course, the magnetic helicity vanishes on the average. However, in the spirit of the Hosking phenomenology of a decay controlled by the conservation of the Hosking integral, it is well possible that even in decaying turbulence, the conservation of magnetic helicity in patches of one sign of magnetic helicity plays an important role in causing the resistively controlled decay speed. Whether or not this is equivalent to talking about reconnection remains an open question. As discussed in Sect. 2, the idea of reconnection in terms of current sheets and plasmoids may not be fully applicable in the context of turbulence, where magnetic structures are more volume filling than in standard reconnection experiments; see Fig. 2. Additional support for a possible mismatch between classical reconnection theory and turbulent decay times comes from our numerical finding that the dependence of $C_{\rm M}$ on Lu seems to be independent of the value of $\mathrm{Pr_M}$; see Fig. 13. More extensive numerical studies with resolutions of 8192^3 meshpoints, which was the resolution needed to see a leveling off in 2–D, might suffice to verify our 2–D findings in the 3–D case.

Our present work motivates possible avenues for future research. One is to do the same for turbulence with a $-\alpha\boldsymbol{u}$ friction term in the momentum equation. Such calculations were already performed by Banerjee & Jedamzik (2004) and the friction term has also been incorporated in the phenomenology of Hosking & Schekochihin (2023). It is to model the drag from photons when their mean-free path begins to exceed the scale $\xi_{\rm M}$. This is the case after the time of recombination, when it contributes to dissipating kinetic energy and leads to a decoupling of the magnetic field. The field then becomes static and remains frozen into the plasma. According to the work of Hosking & Schekochihin (2023), this results in a certain reduction of $C_{\rm M}$ compared to the resistively limited value. Verifying this with simulations would be particularly important.

Another critical aspect to verify is the absence of a dependence of $C_{\rm M}$ on $\mathrm{Pr_M}$ over a broader range of parameter combinations. Given that there are always limitations on the resolution, it may be useful to explore simulations in rectangular domains to cover a larger range of scales. Other possibilities include simulations with time-dependent values of η and ν to obtain a larger separation between $\xi_{\rm M}$ and the dissipation scale near the end of the simulation. However, there is the danger that artifacts are introduced that need to be carefully examined. Ill-understood artifacts can also be introduced by using hyperviscosity and hyperresistivity, which are used in some simulations. For the time being, however, the possibility of a $\mathrm{Pr_M}$ dependence of $C_{\rm M}$ cannot be confirmed from our simulations. Whether or not this automatically rules out reconnection as the reason for a resistively limited value of $C_{\rm M}$, instead of the idea of magnetic helicity conservation in smaller patches, remains uncertain.

As the value of $\mathrm{Pr_M}$ is increased, we also see a systematic increase of the kinetic to magnetic dissipation ratio, $\epsilon_{\rm K}/\epsilon_{\rm M}$. Such a dependence has previously been seen for kinetically dominated forced turbulence, but it is here perhaps for the first time that is has been obtained for magnetically dominated decaying turbulence. While such results may be of interest to the problem of coronal heating, it should be remembered that the present simulations have large plasma betas, i.e., the gas pressure dominates over the magnetic pressure. It would therefore be of interest to check whether the obtained $\mathrm{Pr_M}$-dependence also persists for smaller plasma beta. The restriction to two dimensions has been another computational simplification allowing significantly larger Lundquist numbers to be accessed, but it needs to be checked that the results for $\epsilon_{\rm K}/\epsilon_{\rm M}$ are not very sensitive to this restriction. Comparing the 3–D Runs M1 and M3 of Table 1 with the 2–D Run 2M3 of Table 3, which have $\mathrm{Pr_M}=5$ and similar Lundquist numbers, we see that the 2–D results may overestimate the ratio $\epsilon_{\rm K}/\epsilon_{\rm M}$ by a factor of about two. Future work will need to show whether this can also be confirmed for other parameters.

Acknowledgements. We thank Pallavi Bhat (Bangalore) and David Hosking (Princeton) for detailed comments and suggestions, especially regarding reconnection in the 2–D case. We are also acknowledge inspiring discussions with the participants of the program on "Turbulence in Astrophysical Environments" at the Kavli Institute for Theoretical Physics in Santa Barbara. We are also grateful to Sébastien Galtier, Romain Meyrand, Annick Pouquet, and Alex Schekochihin for their interest in shedding light on the origin of the word anastrophy; see Appendix A. This research was supported in part by the Swedish Research Council (Vetenskapsrådet) under Grant No. 2019-04234, the National Science Foundation under Grant No. NSF PHY-1748958, a NASA ATP Award 80NSSC22K0825, and the Munich Institute for Astro-, Particle and BioPhysics (MIAPbP), which is funded by the Deutsche Forschungsgemeinschaft (DFG, German Research Foundation) under Germanys Excellence Strategy - EXC-2094 - 390783311. We acknowledge the allocation of computing resources provided by the Swedish National Allocations Committee at the Center for Parallel Computers at the Royal Institute of Technology in Stockholm. F.V. acknowledges partial financial support from the Cariplo "BREAKTHRU" funds Rif: 2022-2088 CUP J33C22004310003.

Software and Data Availability. The source code used for the simulations of this study, the Pencil Code (Pencil Code Collaboration et al. 2021), is freely available on `https://github.com/pencil-code/`. The DOI of the code is https://doi.org/10.5281/zenodo.2315093. The simulation setups and corresponding data are freely available on `https://doi.org/10.5531/sd.astro.9` (Brandenburg et al. 2024) and `https://doi.org/10.5281/zenodo.10527437`.

References

Armua, A., Berera, A., & Calderón-Figueroa, J. 2023, Phys. Rev. E, 107, 055206
Banerjee, R. & Jedamzik, K. 2004, Phys. Rev. D, 70, 123003
Batchelor, G. K. 1953, The Theory of Homogeneous Turbulence (Cambridge University Press)
Baym, G., Bödeker, D., & McLerran, L. 1996, Phys. Rev. D, 53, 662
Bhat, P., Zhou, M., & Loureiro, N. F. 2021, Mon. Not. Roy. Astron. Soc., 501, 3074
Bhattacharjee, A., Huang, Y.-M., Yang, H., & Rogers, B. 2009, Phys. Plasmas, 16, 112102
Biskamp, D. & Müller, W.-C. 1999, Phys. Rev. Lett., 83, 2195
Brandenburg, A. 2001, Astrophys. J., 550, 824
Brandenburg, A. 2014, Astrophys. J., 791, 12
Brandenburg, A., Enqvist, K., & Olesen, P. 1996, Phys. Rev. D, 54, 1291
Brandenburg, A. & Kahniashvili, T. 2017, Phys. Rev. Lett., 118, 055102
Brandenburg, A., Kahniashvili, T., Mandal, S., et al. 2017, Phys. Rev. D, 96, 123528
Brandenburg, A., Kahniashvili, T., & Tevzadze, A. G. 2015, Phys. Rev. Lett., 114, 075001
Brandenburg, A., Neronov, A., & Vazza, F. 2024, Datasets of Resistively Controlled Primordial Magnetic Turbulence Decay, doi: 10.5531/sd.astro.9
Brandenburg, A. & Oughton, S. 2018, Astron. Nachr., 339, 641
Brandenburg, A., Rädler, K.-H., Rheinhardt, M., & Subramanian, K. 2008, Astrophys. J. Lett., 687, L49
Brandenburg, A. & Rempel, M. 2019, Astrophys. J., 879, 57
Brandenburg, A., Sharma, R., & Vachaspati, T. 2023, J. Plasma Phys., 89, 905890606
Cheng, B. & Olinto, A. V. 1994, Phys. Rev. D, 50, 2421

Christensson, M., Hindmarsh, M., & Brandenburg, A. 2001, Phys. Rev. E, 64, 056405
Comisso, L. & Bhattacharjee, A. 2016, J. Plasma Phys., 82, 595820601
Comisso, L., Grasso, D., & Waelbroeck, F. L. 2015, Phys. Plasmas, 22, 042109
Comisso, L. & Sironi, L. 2019, Astrophys. J., 886, 122
Craig, I. J. D., Litvinenko, Y. E., & Senanayake, T. 2005, Astron. Astrophys., 433, 1139
Craig, I. J. D. & McClymont, A. N. 1991, Astrophys. J. Lett., 371, L41
Durrer, R. & Caprini, C. 2003, J. Cosmology Astropart. Phys., 2003, 010
Dwivedi, S., Anandavijayan, C., & Bhat, P. 2024, arXiv e-prints, arXiv:2401.01965
Falkovich, G. 1994, Phys. Fluids, 6, 1411
Fyfe, D. & Montgomery, D. 1976, J. Plasma Phys., 16, 181
Galishnikova, A. K., Kunz, M. W., & Schekochihin, A. A. 2022, Phys. Rev. X, 12, 041027
Galsgaard, K. & Nordlund, Å. 1996, J. Geophys. Res., 101, 13445
Galtier, S. & Meyrand, R. 2015, J. Plasma Phys., 81, 325810106
Hatori, T. 1984, J. Phys. Soc. Jpn, 53, 2539
Haugen, N. E. L., Brandenburg, A., & Dobler, W. 2003, Astrophys. J. Lett., 597, L141
Hosking, D. N. & Schekochihin, A. A. 2021, Phys. Rev. X, 11, 041005
Hosking, D. N. & Schekochihin, A. A. 2023, Nat. Comm., 14, 7523
Kahniashvili, T., Tevzadze, A. G., Brandenburg, A., & Neronov, A. 2013, Phys. Rev. D, 87, 083007
Kowal, G., Lazarian, A., Vishniac, E. T., & Otmianowska-Mazur, K. 2009, Astrophys. J., 700, 63
Lazarian, A., Eyink, G. L., Jafari, A., et al. 2020, Phys. Plasmas, 27, 012305
Lazarian, A. & Vishniac, E. T. 1999, Astrophys. J., 517, 700
Liu, Y.-H., Cassak, P., Li, X., et al. 2022, Comm. Phys., 5, 97
Loureiro, N. F., Samtaney, R., Schekochihin, A. A., & Uzdensky, D. A. 2012, Phys. Plasmas, 19, 042303
Neronov, A. & Vovk, I. 2010, Science, 328, 73
Parker, E. N. 1957, J. Geophys. Res., 62, 509
Pencil Code Collaboration, Brandenburg, A., Johansen, A., et al. 2021, J. Open Source Softw., 6, 2807
Pouquet, A. 1978, J. Fluid Mech., 88, 1
Pouquet, A. 1993, Les Houches Session XLVII, 139
Rappazzo, A. F., Dahlburg, R. B., Einaudi, G., & Velli, M. 2018, Mon. Not. Roy. Astron. Soc., 478, 2257
Rappazzo, A. F., Velli, M., Einaudi, G., & Dahlburg, R. B. 2007, Astrophys. J. Lett., 657, L47
Saffman, P. G. 1967, J. Fluid Mech., 27, 581
Schekochihin, A. A. 2022, J. Plasma Phys., 88, 155880501
Schekochihin, A. A., Cowley, S. C., Taylor, S. F., Maron, J. L., & McWilliams, J. C. 2004, Astrophys. J., 612, 276
Sweet, P. A. 1958, in Electromagnetic Phenomena in Cosmical Physics, ed. B. Lehnert, Vol. 6, 123
Tronko, N., Nazarenko, S. V., & Galtier, S. 2013, Phys. Rev. E, 87, 033103
Uzdensky, D. A. & Loureiro, N. F. 2016, Phys. Rev. Lett., 116, 105003
Uzdensky, D. A., Loureiro, N. F., & Schekochihin, A. A. 2010, Phys. Rev. Lett., 105, 235002
Vachaspati, T. 1991, Phys. Lett. B, 265, 258
Vakoulenko, M. O. 1993, J. Plasma Phys., 50, 45
Zhou, H., Sharma, R., & Brandenburg, A. 2022, J. Plasma Phys., 88, 905880602
Zhou, M., Wu, D. H., Loureiro, N. F., & Uzdensky, D. A. 2021, J. Plasma Phys., 87, 905870620
Zrake, J. 2014, Astrophys. J. Lett., 794, L26

Appendix A: Historical note on anastrophy

In recent years, the term anastrophy for the mean squared magnetic vector potential $\langle A_z^2 \rangle$ = const has become increasingly popular (Tronko et al. 2013; Galtier & Meyrand 2015; Zhou et al. 2021; Hosking & Schekochihin 2021; Schekochihin 2022). In the 1970s, it was referred to as mean square vector potential (Fyfe & Montgomery 1976) or as the variance of the magnetic potential (Pouquet 1978). The term anastrophy was first used in the 1987 Les Houches lecture notes by Pouquet (1993), and it was also used by Vakoulenko (1993), but neither of them provided an explanation of its origin.

Annick Pouquet (private communication) informed us now that the word may have been invented by Uriel Frisch and Nicolas Papanicolaou during a meeting on a Winter Sunday in the late 1970s at Saint-Jean-Cap-Ferrat, while she and Jacques Léorat were also present.

The word has Greek roots, where 'strophe' refers to curl or turning, and 'ana' therefore hints at the inverted curl of $\boldsymbol{B}$. This is somewhat reminiscent of the word palinstrophy, which is the mean squared double curl of the velocity, where 'palin' means again. This term was also invented by Frisch and Papanicolaou. The palinstrophy is proportional to the rate of change of enstrophy, i.e., the mean squared vorticity.

Appendix B: Resolving the plasmoid instability

The expected thickness of critical layers, i.e., the smallest thickness of current sheets when they become unstable to the plasmoid instability, is expected to be of the order of $\delta_{\rm c}$; see Sect. 6. To compare this with our 2–D simulations, we show in Fig. 10 visualizations of $J_z(x,y)$ in parts of the full domain with sizes $5\xi_{\rm M} \times 10\xi_{\rm M}$ at times $t = 1$, 10, 100, and 464. Note that $\xi_{\rm M}(t)$ increases with time, so the x and y ranges increase with time too. We see that each panel contains about one pair of current tubes. Furthermore, the other length scales, $L_{\rm c}$ and $\delta_{\rm c}$, increase with time by the same factor, as expected for a self-similar evolution.

At late times, for $t = 100$ and 464, the current sheets are seen to break up into plasmoids. They are obviously better resolved in Run 2m6 with 16384^2 mesh points than in Run 2m5 with only 8192^2 mesh points. At lower resolution, one sees a higher tendency for ringing, i.e., the formation of oscillations on the grid scale, which indicates that the resolution limit has been reached. Nevertheless, Table 3 and Fig. 13 show that, within error bars, the values of $C_{\rm M}$ are similar for the two resolutions.

It is possible that the critical current sheets are not well resolved during a significant fraction of the duration of the simulation. Theoretically, one expects the thinnest sheets to set the reconnection rate, but this is also the place where the value of ${\rm Pr_M}$ matters, because viscosity is unimportant for the larger scales in the plasmoid hierarchy. Therefore, if one does not resolve that sheet, it seems reasonable that one would also not see a dependence on ${\rm Pr_M}$. To check this, we now consider a version of Run 2m2, where the viscosity is ten times larger, which increases ${\rm Pr_M}$ from 10 to 100; see Run 2m6. The result is shown in Fig. B.1. We see that a lower value of Lu for ${\rm Pr_M} = 100$ changes the results in an expected fashion, thus rejecting the possibility that the weak dependence of $C_{\rm M}$ on ${\rm Pr_M}$ was an artifact of having chosen unreliably large values of Lu; compare Runs 2m1 and 2m2 in Fig. B.2.

In the bottom right panel of Fig. B.1, we see the same current sheet that was already presented in Sect. 6 as Fig. 14. However, we also see in Fig. B.1 that there are many other current sheets that are not yet in the process of breaking up.

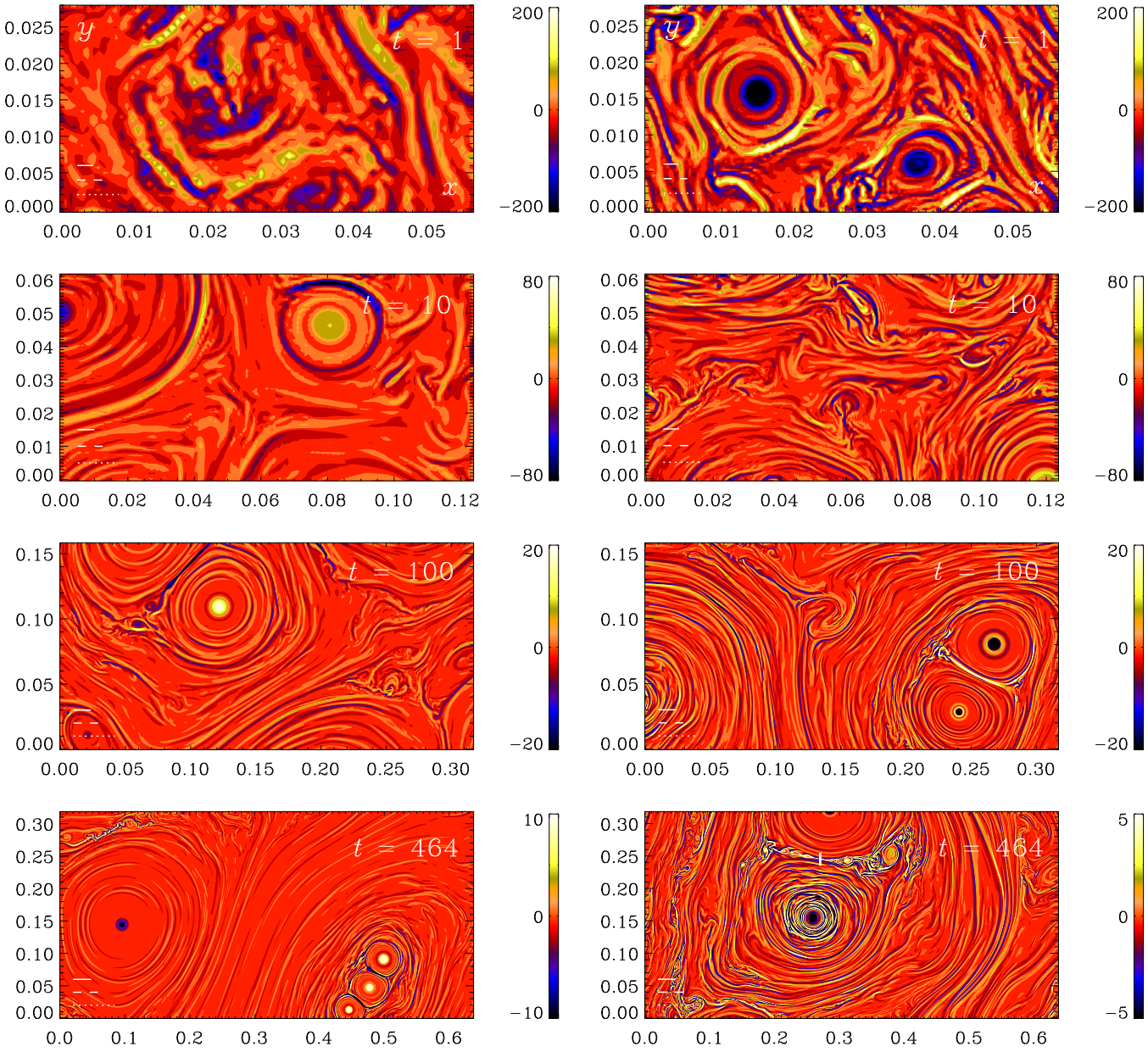

Fig. B.1. Comparisons of visualizations of $J_z(x,y)$ for Runs 2m5 and 2m6 with $\mathrm{Pr_M}=10$ and 8192^2 (left) and 16384^2 (right) mesh points at times $t=1$, 10, 100, and 464. In each panel, the lengths of the dotted, dashed, and solid lines denote the values of ξ_M, $5\,L_\mathrm{c}$, and $500\,\delta_\mathrm{c}$. Note that the bottom right panel shows the same current sheet that was presented in Fig. 14 as a blow-up. The thick white line in that panel at $(x,y)=(0.27,0.25)$ marks the location of the cross-section shown in Fig. 15.

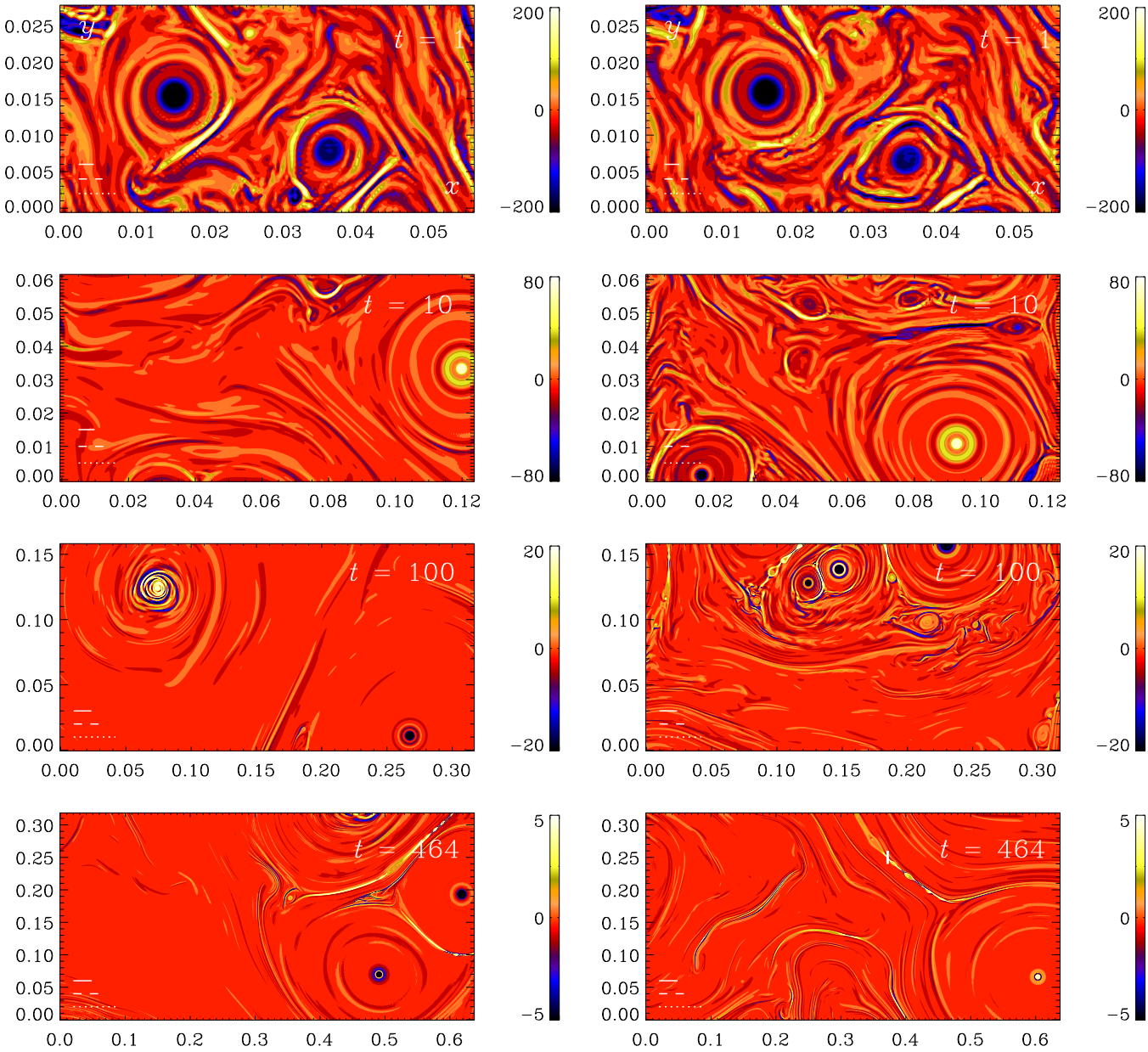

Fig. B.2. Similar to Fig. B.1 but for Run 2m1 with $\mathrm{Lu} = 75,000$ (left) and Run 2m2 with $\mathrm{Lu} = 182,000$ (right) using $\mathrm{Pr_M} = 100$ and 16384^2 mesh points in both cases. The thick white line in the bottom right panel at $(x, y) = (0.37, 0.25)$ marks the location of the cross-section shown in Fig. 15.